URSI GASS 2020, Rome, Italy, 29 August - 5 September 2020

The photoelectron driven upper hybrid instability as the cause of 150 km echoes

William J. Longley*(1,2), Meers M. Oppenheim(3), Nick M. Pedatella(4), and Yakov S. Dimant(3)
(1) Department of Physics and Astronomy, Rice University, Houston, TX, USA
(2) University Corporation for Atmospheric Research, Boulder, CO, USA
(3) Center for Space Physics, Boston University, Boston, MA, USA
(4) High Altitude Observatory, National Center for Atmospheric Research, Boulder, CO, USA

Abstract

150 km echoes are strong, coherent echoes observed by equatorial radars looking close to perpendicular to the Earth's magnetic field. Observations over a day show a distinct necklace pattern with the echoes descending from 170 km at sunrise to 130 km at noon, before rising again and disappearing overnight. This research shows that the upper hybrid instability will convert photoelectron energy into plasma wave energy through inverse Landau damping. Using parameters from a WACCM-X simulation, the upper hybrid wave growth rates over a day show a nearly identical necklace pattern, with bands of positive growth rate following contours of the plasma frequency. Small gaps in altitude with no echoes are explained by thermal electrons Landau damping the instability in locations where the upper hybrid frequency is a multiple of the gyrofrequency. This theory provides a mechanism that likely plays a crucial role in solving a long-standing mystery on the origin of 150 km echoes.

1 Introduction

Early observations at Jicamarca Radio Observatory found strong radar echoes at altitudes between 130 and 170 km [1], [2]. Without an easily identified source, these observations received the epithet of "150 km echoes," and continued to be observed and utilized despite having no understanding of their generation [3]. Figure 1 shows some typical observations at the 50 MHz Jicamarca radar. Every day the echoes start around 160 km at sunrise, then appear to descend to a minimum altitude of ~130 km before rising in altitude again. This descending pattern along with a set of distinct altitude gaps in the echoes creates a distinctive "necklace" pattern of the echoes. Other equatorial radars that transmit between 30-50 MHz see these same echoes, although the daily pattern depends on the radar's sensitivity [4].

Recently, Oppenheim and Dimant [5] provided the first physical explanation of the source for 150 km echoes: high frequency waves generated by a photoelectron bump-on-tail. The kinetic simulations in [5] show that a photoelectron bump-on-tail is unstable in a magnetized plasma, which drives high frequency electron modes that then decay nonlinearly into ion waves that can be measured by radars. Photoelectron peaks at 5 eV and 22-27 eV are observed between 120-180 km during the day [6], [7], further justifying their connection with 150 km echoes. The photoelectron dependence in the [5] model also explains several key features of 150 km echoes: why they are not observed at night, their enhancement during solar flares [8], [9], and suppression during eclipses [4]. In this research we develop the kinetic theory behind photoelectron driven waves, showing that 150 km echoes are likely caused by the photoelectron driven upper hybrid instability.

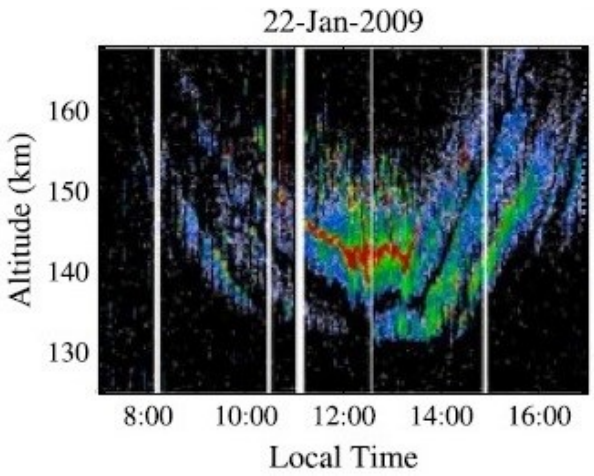

Figure 1. Measurement of 150 km echoes at Jicamarca from Chau and Kudeki [10]. The color scale shows the received power of the radar in dB.

The kinetic theory for photoelectron induced instabilities in the valley region ionosphere (defined roughly as 120 to 200 km altitude) is developed in [11], and further expanded in [12]. One of the instabilities analyzed in [11] is the upper hybrid instability, which is generated by inverse Landau damping of photoelectrons. [12] calculated positive growth rates in the valley region but did not show how the prevalence of the instability can evolve over the day. The goal of this research is to use ionospheric parameters from WACCM-X simulations in order to calculate where the upper hybrid instability will occur over a day. In the next section the derivation of the upper hybrid instability is outlined, along with a necessary expansion on the theory for regions of the ionosphere where the upper hybrid frequency is a multiple of the gyrofrequency, which allows for thermal electrons to Landau damp the instability.

2 The Upper Hybrid Instability

The kinetic instability of interest is the upper hybrid (UH) instability, which is driven by inverse Landau damping (including cyclotron damping) of a photoelectron bump-on-tail. The UH instability was originally derived in [11] for applications to the valley region, and this section expands the theory to include Landau damping by thermal electrons. The instability drives waves at frequencies comparable to the electron plasma frequency and therefore the dynamics are described by the electron Boltzmann equation with a BGK collision operator to model the collisions between electrons and neutrals.

The standard solution of the Boltzmann equation for waves propagating with $k_\parallel \ll k_\perp$ is the upper hybrid mode:

$$\omega_{UH}^2 = \omega_p^2 + \Omega^2. \quad (1)$$

The primary damping of the upper hybrid wave is through electron neutral collisions, with a damping rate of [12]

$$\gamma_\nu = -\nu_m \frac{\omega_{UH}^2 + \Omega^2}{2\omega_{UH}^2}. \quad (2)$$

Including a photoelectron population in the solution of the Boltzmann equation leads to an additional imaginary component of the frequency [11]:

$$\gamma_{ph} = \frac{\pi^2 \omega_p^4}{k_\parallel k^2 n_0} \sum_n \left(\frac{n\Omega}{\omega_{UH}}\right) \int_0^\infty dv_\perp J_n^2(b) \left[\frac{\partial f_{0h}}{\partial v_\perp}\right]_{v_\parallel, res}. \quad (3)$$

In equation (3) the derivative of the photoelectron distribution, f_{0h}, is evaluated at the resonance condition $v_\parallel = (\omega_{UH} - n\Omega)/k_\parallel$. If this derivative is positive, as happens with a bump-on-tail, then the photoelectron population will inverse Landau damp and upper-hybrid waves will be driven with a growth rate of γ_{ph}.

In [11] and [12] the only damping for the upper hybrid waves is the electron-neutral collisional damping, and the expression for the dielectric function is only valid when $\omega_{UH} - n\Omega \gg k_\parallel v_{th}$. Since we are interested in calculating the total growth rate across the whole valley region, the upper hybrid frequency will pass through a region where $\omega_{UH} \approx n\Omega$, and the dielectric function needs to be reevaluated. Reevaluating the dielectric function without the assumption of $\omega_{UH} - n\Omega \gg k_\parallel v_{th}$ produces another damping term that can suppress the instability. This additional damping is caused by thermal electrons Landau damping the wave, and that damping rate is

$$\gamma_{LD} = -\frac{\sqrt{\pi}\omega_p^4 a_r \exp(-y_r^2)}{4\Omega^2 k_\parallel v_{th}}, \quad (4)$$

where $y_r = (\omega_{UH} - r\Omega)/k_\parallel v_{th}$. This damping rate becomes important when $y_r < 1$, since the Landau resonance is at a $v_\parallel$ small enough to occur in the bulk of the thermal electron distribution.

The growth and damping rates of the UH instability are evaluated using a drifting Maxwellian for the photoelectron distribution. Rocket measurements in the valley region by [7] show a bite out in the photoelectron distribution at 2.3 eV due to a collisional resonance between electrons and molecular Nitrogen, which creates a peak in the distribution at approximately 5 eV. The measurements using the AE-E satellite in [6] show several photoelectron peaks between 22-27 eV caused by He II solar emission lines. To model both of these photoelectron peaks the drifting Maxwellian distribution is evaluated with peak energies of $E_0 = 5$ eV and $E_0 = 25$ eV. This idealized distribution is assumed at all altitudes and times so that the effects of the background ionosphere on the instability can be studies in isolation. Future work will examine how the distribution's altitude and time dependence, fine structuring, and exact form at 2.3 eV can affect the upper hybrid instability.

3 WACCM-X Simulations

The growth and damping rates of the upper hybrid instability have a strong dependence on the thermal electron density and temperature, as well as the neutral density and composition. The WACCM-X model is used to obtain reasonable values of these parameters between 100-200 km over the course of a day. WACCM-X extends from the surface to ~600 km, and incorporates the necessary chemical, dynamical, and physical processes to model the troposphere, stratosphere, mesosphere, thermosphere and ionosphere. Constant solar and geomagnetic activity is used, specified as 105 sfu and a Kp of 1.0, respectively. The neutral and ionosphere parameters at the location of Jicamarca on January 28 are used to calculate the instability growth and damping rates. This is considered as a representative January day since the day-to-day variations in the valley region are small under fixed solar and geomagnetic conditions.

4 Results

Calculating the total growth rate for the upper hybrid instability over the course of a single day at Jicamarca gives the results shown in Figure 2. This figure compares the total growth rate to the specific contributions: the instability growth rate in equation (3), the collisional damping rate in equation (2), and the thermal electron Landau damping rate in equation (4). The growth and damping rates in Figure 2 are evaluated using only the 5 eV photoelectron population, with a wavelength of $\lambda = 20\ cm$, and an aspect angle of $\alpha = 2°$ (defined where 0° corresponds to $k_\parallel = 0$). The undamped instability shows several layers in the ionosphere where the upper hybrid frequency meets the inverse Landau damping criteria where derivative of the 5 eV bump is positive at the resonance condition $v_\parallel = (\omega_{UH} - n\Omega)/k_\parallel$. The generation of the instability at night only occurs because a constant photoelectron distribution is always assumed, despite photoelectron production ceasing at night. The instability is generated at altitudes below 130 km, but when collisional damping is added the instability is suppressed at lower altitudes. Figure 2 also shows the Landau damping by thermal electrons is significant enough to suppress the instability in narrow layers.

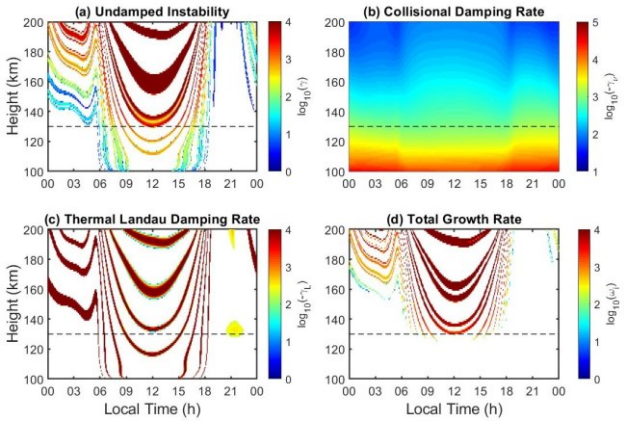

Figure 2. Contribution of different terms to the UH instability, with $\boldsymbol{E_0 = 5\ eV}$, $\boldsymbol{\lambda = 20\ cm}$, and $\boldsymbol{\alpha = 2°}$. The horizontal dashed line corresponds to 130 km altitude.

The dependence of the upper hybrid instability on the aspect angle and photoelectron energy is shown in Figure 3. For all combinations of photoelectron energy E_0, and aspect angle α, the instability is suppressed below 130 km due to collisional damping. The difference between a 5 eV and 25 eV photoelectron bump is also seen, as each energy has a different resonance condition where inverse Landau damping can occur. We also see that larger aspect angles favor the instability, which comes from the growth rate being inversely proportional to $k_\parallel$. However, at large enough $k_\parallel$ this trend will reverse, as the criteria for thermal electron Landau damping, $\omega_{UH} - n\Omega < k_\parallel v_{th}$, is more easily met for large $k_\parallel$. The instability will only occur at aspect angles close to 0°, though at $\alpha = 0°$ inverse Landau damping is not possible, and the instability cannot occur.

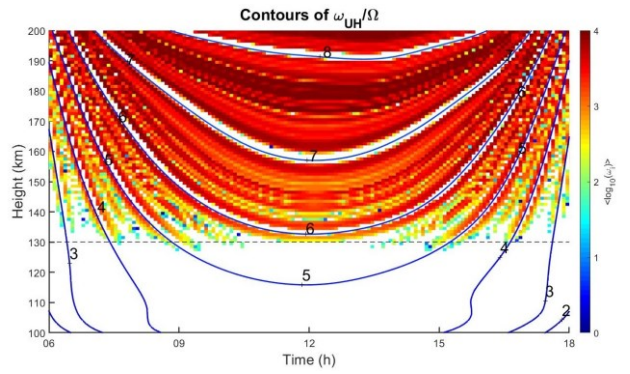

Figure 3. The summation of growth rates for a variety of wavelengths. The colored regions show where the upper hybrid instability will occur in the ionosphere. The contours of $\boldsymbol{\omega_{UH}/\Omega}$ are plotted as well, showing the gaps in the instability occur where $\boldsymbol{\omega_{UH} \approx n\Omega}$ and Landau damping by thermal electrons suppresses the instability.

Figure 2 shows that in narrow bands the thermal electron Landau damping can suppress the instability. To further investigate this, we calculate the growth rates for both photoelectron peaks at $\alpha = 2°$, with $\lambda = 20, 22.5, 25, 27.5, \text{and } 30\ cm$, and add all of the growth rates together. Figure 3 shows this total growth rate, which has the effect of showing all of the regions in the ionosphere where some combination of E_0 and λ is able to drive the instability while also allowing the possibility of one photoelectron peak to Landau damp the instability being generated by the other peak. The thermal Landau damping suppresses the instability for any combination of E_0, λ and α, which creates altitude gaps where $\omega_{UH} \approx n\Omega$ (contours of ω_p/Ω lie just above the gaps). A similar plot without the thermal Landau damping term shows no such gaps in the instability.

5 Discussion and Summary

The regions of the ionosphere where the upper hybrid instability will occur correspond well to the regions where 150 km echoes are observed. The photoelectron dependence of the instability explains why 150 km echoes are not observed at night. The collisional damping of the instability sets a lower boundary at 130 km, which is the same as the observations in Figure 1 from [10]. The gaps in the instability occur where $\omega_{UH} \approx n\Omega$ and thermal Landau damping suppresses the instability. These gaps in the instability correspond exactly to the observations in [13] (see also [14]), which took ionosonde measurements at the same time Jicamarca observed 150 km echoes and calculated the gaps at altitudes where $\omega_{UH} \approx n\Omega$. The growth rate varies linearly with both photoelectron and thermal electron density, which both increase during a solar flare. Therefore, the instability is enhanced during solar flares and can overcome the collisional damping at lower altitudes, which directly explains the observations of 150 km echoes descending in altitude during a solar flare [8], [9].

The upper hybrid instability explains many of the observed features in 150 km echoes, but there are still some features that are not reproduced. The first is that the instability is predicted at all altitudes between 130-200 km. In observations the upper boundary of the echoes at noon is approximately 150 km. The lack of this upper boundary can be explained by two effects. First, the photoelectron production diminishes above 180 km which smooths out the bump-on-tail feature of the distribution and suppresses the instability [6], [7]. The second is that at these higher daytime altitudes the thermal electron temperature rises significantly. This higher temperature increases the gyroradius, and the quantity $k_\perp^2 \bar{\rho}_e^2$ is no longer small enough to discard higher order terms. The full solution of the upper hybrid instability at higher altitudes will therefore need to include these finite Larmor radius effects to be fully valid. Other features not reproduced are the small-scale structuring of the echoes [8], [14], which occur on scales smaller than the 5-minute, ~4 km resolution of WACCM-X.

The upper hybrid instability occurs at high frequencies and short wavelengths. However, the radars that observe 150 km echoes have Bragg scattering wavelengths of 3-6 meters, and observe Doppler shifts associated with low

frequency ion waves. For the upper hybrid instability to cause 150 km echoes, some mechanism must cascade the energy from the electron scale waves to the observed ion scale waves. The kinetic simulations in [5] showed that this mode conversion does occur in a photoelectron driven instability, but the exact mechanism is not explained. Weak turbulence theory may explain this mode conversion, and a wavenumber matching condition in weak turbulence theory could also explain the lack of observations at the higher frequency ALTAIR radar.

6 Acknowledgements

This research was supported by the NASA Living With a Star Jack Eddy Postdoctoral Fellowship Program, administered by UCAR's Cooperative Programs for the Advancement of Earth System Science (CPAESS) under award #NNX16AK22G. This work was supported by NSF grant AGS-1755350. This material is based upon work supported by the National Center for Atmospheric Research, which is a major facility sponsored by the National Science Foundation under Cooperative Agreement 1852977. WACCM-X is available at http://www.cesm.ucar.edu. The results from WACCM-X and the code used in this research are available on Zenodo at doi:10.5065/D6RX99HX. We thank the International Space Science Institute for facilitating discussions related to this research as part of the International Team "An Exploration of the Valley Region in the Low Latitude Ionosphere: Response to Forcing from Below and Above and Relevance to Space Weather".

7 References

[1] B. B. Balsley (1964), "Evidence of a stratified echoing region at 150 kilometers in the vicinity of the magnetic equator during daylight hours," *J. Geophys. Res.*, 69 (9), doi:10.1029/JZ069i009p01925.

[2] E. Kudeki, and C. D. Fawcett (1993), "High resolution observations of 150 km echoes at Jicamarca," *Geophys. Res. Lett.*, *20*, 1987–1990, doi:10.1029/93GL01256

[3] J. L. Chau and R. F. Woodman (2004), "Daytime vertical and zonal velocities from 150-km echoes: Their relevance to F-region dynamics," *Geophys. Res. Lett*., 31, L17801, doi:10.1029/2004GL020800.

[4] A. K. Patra, P. Pavan Chaitanya, and D. Tiwari (2011), "Characteristics of 150 km echoes linked with solar eclipse and their implications to the echoing phenomenon", *J. Geophys. Res.,* 116, A05319, doi:10.1029/2010JA016258.

[5] M. M. Oppenheim and Y. S. Dimant (2016), "Photoelectron-induced waves: A likely source of 150 km radar echoes and enhanced electron modes," *Geophys. Res. Lett.*, 43, 3637–3644, doi:10.1002/2016GL068179.

[6] J. S. Lee, J. P. Doering, T. A. Potemra, and L. H. Brace (1980), "Measurements of the ambient photoelectron spectrum from Atmosphere Explorer: I. AE-E measurements below 300 km during solar minimum conditions," *Planet. Space Sci*., 28, 947–971, doi:10.1016/0032-0633(80)90058-6.

[7] W. J. McMahon and L. J. Heroux (1983), "The 2- to 5-eV energy spectra of thermospheric photoelectrons: Measurements in apparent conflict with theory," *J. Geophys. Res.,* 88, doi:10.1029/JA088iA11p09249.

[8] P. Reyes (2012), "Solar Flare Effects Observed Over Jicamarca During MST-ISR Experiments" M. S. dissertation, University of Illinois at Urbana-Champaign. Retrieved at hdl.handle.net/2142/31196

[9] N. M. Pedatella, J. L. Chau, J. Vierinen, L. Qian, P. M. Reyes, E. Kudeki, et al. (2019), "Solar flare effects on 150-km echoes observed over Jicamarca: WACCM-X simulations," *Geophys. Res. Lett*., 46, 10951– 10958. doi:10.1029/2019GL084790

[10] J. L. Chau and E. Kudeki (2013), "Discovery of two distinct types of equatorial 150 km radar echoes," *Geophys. Res. Lett.*, *40*, 4509–4514, doi:10.1002/grl.50893.

[11] B. Basu, T. Chang, and J. R. Jasperse (1982), "Electrostatic plasma instabilities in the daytime lower ionosphere," *Geophys. Res. Lett.*, *9*, 68–71, doi:10.1029/GL009i001p00068.

[12] J. R. Jasperse, B. Basu, J. M. Retterer, D. T. Decker, and T. Chang (1995), "High frequency electrostatic plasma instabilities and turbulence layers in the lower ionosphere", in *Space Plasmas: Coupling Between Small and Medium Scale Processes*, vol. 86, edited by M. Ashour-Abdalla, T. Chang, and P. Dusenbery, pp. 77, AGU, Washington, D. C.

[13] G. A. Lehmacher, H. Wu, E. Kudeki, P. M. Reyes, D. L. Hysell, and M. Milla (2020), "Height variation of gaps in 150-km echoes and Whole Atmosphere Community Climate Model electron densities suggest link to upper hybrid resonance," *J. Geophys. Res.: Space Physics*, 125. doi:10.1029/2019JA027204

[14] P. Reyes (2017). "Study of Waves Observed in the Equatorial Ionospheric Valley Region using Jicamarca ISR and VIPIR Ionosonde," Ph. D. dissertation, University of Illinois at Urbana-Champaign. Retrieved from hdl.handle.net/2142/98349